Color Imaging Arithmetic: Physics ∪ Math > Physics + Math

Gaurav Sharma*

University of Rochester, Department of Electrical and Computer Engineering,
Rochester, NY 14627-0126, USA
{gaurav.sharma}@rochester.edu
http://www.ece.rochester.edu/~gsharma/

Abstract. Color imaging devices for capture, display, and user interaction commonly form the physical interface by which we connect to the digital cyber-world. Because these devices bridge the physical and the electronic worlds, elegant and effective solutions to problems in color imaging can often be found by the synergistic combination of physical intuition with the mathematical tools of signal and image processing. In this paper, we support this claim using case studies drawn from our past research in color imaging. For each of the illustrative examples, we highlight how the blend of physical insight and mathematical modeling, offer in the combination, advantages significantly greater than would be estimated as the sum of the individual parts, thereby justifying the title for this paper.

1 Introduction

We live in a world governed by the laws of physics. The codification of the physical laws in the form of quantitative mathematical relations, not only aids us in developing a better understanding of the world, but also provides a potent tool for solving problems that may sometimes appear insurmountable at the outset. Newton's laws of motion represent what is, perhaps, the best known example of this philosophical assertion. The mathematical equations representing Newton's laws, arm us with the ability to to quantitatively model interactions between elements in a physical system. This ability allows us to engineer solutions to a variety of problems, including several problems where the complexity can be daunting. For instance, using the laws of motion, we can develop propulsion and control systems for space craft that can undertake inter-planetary travel and allow us to explore our solar system. Also, equally significantly, the quantitative modeling using Newton's laws, can also, on occasion, surprise us by enabling solutions to problems that we may intuitively consider infeasible under a less than thorough first consideration. An example is the inverted pendulum [4] problem, where the a pole mounted with a pivot on a cart can be balanced in an unstable upright position by using an appropriate feedback control methodology. For this

* Invited paper.

R. Schettini, S. Tominaga, and A. Trémeau (Eds.): CCIW 2011, LNCS 6626, pp. 31–46, 2011.
© Springer-Verlag Berlin Heidelberg 2011

latter category of problems, the physical understanding and the mathematical modeling offer in the combination, advantages significantly greater than would be estimated as the sum of the individual parts. In a mathematical play on the words of the common saying "The whole is greater than the sum of the parts," we denote this synergistic combination by the inequality Physics $\cup$ Math $>$ Physics + Math. The illustration of this philosophical theme in the context of color imaging systems is the central objective of this paper.

Color imaging systems handle the capture of physical scenes and the reproduction of images on physical devices, commonly serving as the interface between the tangible physical world and the electronic world that operates on mathematical representations. Therefore, the Physics $\cup$ Math $>$ Physics + Math aphorism rings particularly true for a number of problems in color imaging systems. In this paper, we substantiate this assertion by highlighting specific examples of problems in color imaging for which the combination of physical insight, mathematical tools, and engineering ingenuity leads to particularly elegant and effective solutions.

The rest of this paper is organized as follows. In Section 2, we briefly review colorimetric representations with the dual objectives of introducing relevant notational conventions and to remind our readers that in color imaging the synergistic union of physics and mathematics can be traced back in time to the very the origins of color science. We then bolster the central assertion of the paper by providing, as evidence, two case studies drawn from our research in color imaging, in each case highlighting how the combination of physical modeling/insight with mathematical analysis enables a solutions that each of these tools alone is unable to address adequately. The examples cover two very different applications, the first dealing with numerical metrics for the evaluation of the fidelity of color recording devices and the second addressing the estimation of four separate halftone printing channels from a conventional three channel scan, applied in the specific context of extending phase modulation halftone watermarks to color. We conclude the paper with a summary and a discussion and prognosticate that the harmonious union of Physics and Mathematics will continue to be a happy one in the domain of color imaging.

2 The Union of Physics and Math in Fundamental Color Science

The origins of present day color science can be traced back to the early experiments conducted by the physicists Young, Helmholtz, and Maxwell [9, 14, 15, 29]. These experiments demonstrated that it is possible to produce a color match for a given stimulus by additively combining three light sources and that, in general, fewer than three sources do not suffice for this purpose. The formulation of theories for color perception based on these physical observations *and* the codification of these theories in the form of abstract mathematical relations, exemplified by Grassman's laws of color matching [6], are key ingredients of modern color science. Once mathematical models are available for the physical

phenomena, they enable powerful and novel engineering applications that would otherwise be infeasible. In particular, *colorimetry*, i.e. the science of color measurement and representation, arises directly from the incorporation of the insight from (psycho)-physical experiments on color matching within the mathematical framework of linear vector spaces [2, 3, 24, 28]. Specifically, for instance, colorimetry allows us to specify the color of an object using the so-called CIE XYZ tristimulus values [1], given by

$$\mathbf{t} = \mathbf{A}^T \mathrm{diag}(\mathbf{l})\mathbf{r} = \mathbf{A}_\mathbf{L}^T \mathbf{r}, \tag{1}$$

where spectra are represented as $N \times 1$ vectors with a suitably chosen number of samples, N, and in this discrete format, $\mathbf{r}_{N\times 1}$ denotes the spectral reflectance of the object[1], $\mathbf{l}_{N\times 1}$ the spectral power distribution of the illuminant, $\mathbf{A}_{N\times 3}$ the matrix whose 3 columns form the X, Y, and Z, color matching functions, respectively, that characterize the observed psycho-physical color matches, $\mathrm{diag}(\mathbf{x})$ denotes the square diagonal matrix obtained by placing the elements of the vector $\mathbf{x}$ along the diagonal of an otherwise zero square matrix, and $\mathbf{A}_\mathbf{L} \stackrel{\mathrm{def}}{=} \mathrm{diag}(\mathbf{l})\mathbf{A}$ [21, 24].

Once constructed, the framework of colorimetry, suitably augmented, enables a vast array of color imaging applications, spanning the entire gamut from capture, processing, display, and print. For instance, under identical viewing contexts, the color corresponding to a reflectance $\mathbf{r}_1$ can be matched by producing a reflectance $\mathbf{r}_2$, which although spectrally different from $\mathbf{r}_1$, matches in CIE XYZ tristimulus values, i.e.

$$\mathbf{t}_1 \stackrel{\mathrm{def}}{=} \mathbf{A}^T \mathrm{diag}(\mathbf{l})\mathbf{r}_1 = \mathbf{t}_2 \stackrel{\mathrm{def}}{=} \mathbf{A}^T \mathrm{diag}(\mathbf{l})\mathbf{r}_2. \tag{2}$$

The reflectance $\mathbf{r}_2$ is then said to be a *metamer* of the reflectance $\mathbf{r}_1$ (under the illuminant $\mathbf{l}$). The framework can be and is routinely used to obtain reproductions. Under a chosen illumination $\mathbf{l}$, a colorimetrically matched print for a painting, can be obtained, for instance, by selecting for a spatial location in the painting with reflectance $\mathbf{r}_1$, a corresponding reflectance $\mathbf{r}_2$ for the reproduction that satisfies (2). Specifically, if $\mathbf{r}_2 \stackrel{\mathrm{def}}{=} \mathbf{r}_2(\mathbf{v})$ is the output of a color reproduction device with k-dimensional control values $\mathbf{v} = [v_1, v_2, \ldots v_k]^T$, the objective becomes the determination of control values that achieve the match in (2) or the closest approximation thereof under the trade-off imposed by gamut limitations. For our purposes here, the original can also be described, instead of spectra, by a more condensed tristimulus representation, which forms the basis underlying most representations of color images.

The novelty and elegance of colorimetry are sometimes lost on us because its use is now common-place in color imaging. To regain an appreciation, we need to only recognize that without the underlying framework of colorimetry, the metameric matches that one relies on in all of color reproduction would require a cumbersome process of matching by trial and error, analogous to what one may use in the kitchen in order to construct a recipe for matching the taste for a dish obtained from a restaurant!

[1] Colorimetry for transmissive and emissive objects can be similarly defined.

3 Figures of Merit for Color Recording Devices

As our first case study, we use our work on developing figures of merit for the evaluation of color recording devices [25]. Scanners and digital cameras are commonly used for recording color images. These devices would, in an ideal setting, report exact colorimetric values corresponding to the spectra that are incident upon their sensors. In practice, however, the accuracy of these devices is limited due to manufacturing limitations and unavoidable noise in the recordings. Consequently, for the purposes of design, a quality factor or figure of merit is desirable that characterizes their color accuracy. For our exposition, we consider the specific case of a scanner based capture, the digital camera scenario can be obtained via a straightforward generalization, albeit with key differences in the formulation that address the fact that the illumination is external to the camera.

Analogous to (1), scanner measurements of the object with reflectance $\mathbf{r}$, with a K channel scanner can be modeled as,

$$\mathbf{t}_s(\mathbf{r}) = \mathbf{M}^T \mathrm{diag}(\mathbf{l}_s)\mathbf{r} + \boldsymbol{\eta} \ = \mathbf{G}^T\mathbf{r} + \boldsymbol{\eta} \ , \tag{3}$$

where $\mathbf{t}_s(\mathbf{r})$ is a $K \times 1$ vector of scanner measurements, $\mathbf{M}$ is the $N \times K$ matrix of scanner filter transmittances (including detector sensitivity and the transmittance of the scanner optical path), $\mathbf{l}_s$ is the $N \times 1$ vector representing the scanning illuminant spectrum, $\boldsymbol{\eta}$ is the $K \times 1$ measurement noise vector, and $\mathbf{G} = \mathrm{diag}(\mathbf{l}_s)\mathbf{M}$.

Colorimetric information must be estimated from the scanner recordings by means of a scanner calibration transform. Since both (3) and (1), represent linear measurement models, a linear calibration transform is mathematically justified, a fact that is also borne out by empirical evaluations [25]. Denoting the scanner calibration transform by a 3×3 matrix $\mathbf{B}$, the estimated tristimulus values from the scanner measurements can be mathematically formulated as

$$\mathbf{t}(\hat{\mathbf{r}}) = \mathbf{B}\mathbf{t}_s(\mathbf{r}), \tag{4}$$

where the transformation $\mathbf{B}$ is determined so as to minimize the color error, exact details of which we will consider in the sequel.

A useful metric for design purposes is the average magnitude of the perceived color difference between the true color $\mathbf{t}(\mathbf{r})$ and the estimate $\hat{\mathbf{t}}(\mathbf{r})$. We formulate this metric mathematically as

$$\epsilon(\mathbf{A}_L, \mathbf{G}, \mathbf{B}) = E\left\{ \left\| \mathcal{F}(\mathbf{t}(\mathbf{r})) - \mathcal{F}(\hat{\mathbf{t}}(\mathbf{r})) \right\|^2 \right\}, \tag{5}$$

where $E\{\ \}$ denotes the expectation over the ensemble of scanned objects, $\mathcal{F}()$ is a 3×3 (possibly nonlinear) transformation of the tristimulus values into a perceptually uniform color space such as CIELAB, and $\|\cdot\|$ denotes the Euclidean vector norm [5].

The above error metric quantifies the performance of a scanner "specified by" $\mathbf{G}$ when the transformation $\mathbf{B}$ is used in (4). An error metric for the scanner

alone can be obtained by replacing the generic transformation, $\mathbf{B}$, with the optimal transformation that minimizes the error. However, such an error metric is not readily computable since the optimal transformation cannot be determined in closed form for a general non-linear transformation, $\mathcal{F}()$. If the transformation $\mathcal{F}()$ is differentiable, with continuous first partial derivatives, a first order Taylor series provides a fairly accurate locally linear approximation for $\mathcal{F}()$. If $\left\|\mathbf{t}(\mathbf{r}) - \hat{\mathbf{t}}(\mathbf{r})\right\|$ is small over the scanned ensemble, as it should be for a well-designed scanner, this first order Taylor series can be used to approximate the error metric in (5) by the expected mean-squared linearized color error,

$$\epsilon(\mathbf{A}_L, \mathbf{G}, \mathbf{B}) \approx \epsilon_l(\mathbf{A}_L, \mathbf{G}, \mathbf{B}) = E\left\{\left\|J_{\mathcal{F}}(\mathbf{t}(\mathbf{r}))\ \left(\mathbf{t}(\mathbf{r}) - \hat{\mathbf{t}}(\mathbf{r})\right)\right\|^2\right\}, \tag{6}$$

where $J_{\mathcal{F}}(\mathbf{t}(\mathbf{r}))$ denotes the Jacobian matrix [13] of the transformation $\mathcal{F}()$ at $\mathbf{t}(\mathbf{r})$.

The local linearization offers the advantage that the optimal scanner calibration transformation $\mathbf{B}_{opt}(\mathbf{A}_L, \mathbf{G})$ that minimizes the linearized perceptual color error metric in (6) can be computed in closed form(see [25, 27] for details). The minimum mean-squared linearized color error obtained using the optimal transformation can then be written as,

$$\xi(\mathbf{A}_L, \mathbf{G}) = \epsilon\left(\mathbf{A}_L, \mathbf{G}, \mathbf{B}_{opt}(\mathbf{A}_L, \mathbf{G})\right) \tag{7}$$

which serves as a useful error metric for evaluating the scanner sensitivity $\mathbf{G}$. Through some algebraic manipulation, we can express this error metric in the form

$$\xi(\mathbf{A}_L, \mathbf{G}) = \alpha(\mathbf{A}_L) - \tau(\mathbf{A}_L, \mathbf{G}), \tag{8}$$

where we refer the reader to [25] for details, only observing here that the terms satisfy $0 \leq \tau(\mathbf{A}_L, \mathbf{G}) \leq \alpha(\mathbf{A}_L)$. As a consequence, we can interpret $\alpha(\mathbf{A}_L)$ as the average "color" energy in a spectrum from the spectral ensemble in perceptually uniform color units and $\tau(\mathbf{A}_L, \mathbf{G})$ as the part of this energy that is recoverable from measurements made with the scanner specified by $\mathbf{G}$ (at the given noise level). Hence, the ratio,

$$q_{\mathcal{F}}(\mathbf{A}_L, \mathbf{G}) = \frac{\tau(\mathbf{A}_L, \mathbf{G})}{\alpha(\mathbf{A}_L)}, \tag{9}$$

defines a normalized *figure of merit* (FOM) for the color scanner, where the subscript $\mathcal{F}$ has been added to explicitly indicate the dependence on the transformation $\mathcal{F}()$ (which was implicit in the earlier expressions). The normalization ensures that the figure of merit is bounded between 0 and 1 with $q_{\mathcal{F}}(\mathbf{A}_L, \mathbf{G}) = 1$ representing a "perfect" color scanner whose error metric is zero.

The figure of merit of (9) represents, within a common mathematical framework, a number of alternative metrics that can be obtained by a judicious choice of the transformation $\mathcal{F}()$ and assumptions on the ensemble of spectra over which the expectation in (6) is computed and the statistics of the measurement noise [25]. Specifically, a powerful FOM is obtained by using as the color

space transformation $\mathcal{F}()$ the transformation from CIE XYZ in to the (approximately) perceptually uniform CIELAB color space [1, 28], which we refer to as the comprehensive FOM. We also consider simpler alternatives that have been used in prior designs: 1) A CIE XYZ *mean-squared error* (MSE) based FOM obtained by using the identity mapping for the color space transformation $\mathcal{F}()$, 2) An orthogonal tristimulus FOM which uses a linear transformation $\mathbf{F}_o$ for the transformation $\mathcal{F}()$, in order to ensure that color errors in (6) are computed within an orthonormal tristimulus color space instead of the highly correlated CIE XYZ space, and 3) A perceptual measure of goodness that ignores the noise (by assuming its amplitude is zero), otherwise utilizes the transformation from CIE XYZ in to the (approximately) perceptually uniform CIELAB color space for the color space transformation $\mathcal{F}()$.

To highlight the utility of the framework, we show in Fig. 1 a subset of the results from [25]. The figure compares the comprehensive FOM against the three other alternative FOMs listed in the preceding paragraph by examining the relationship between the FOM and the average $\triangle E^*_{ab}$ error over a representative ensemble of scanner target reflectances for a number of scanner sensitivities determined by a parametrized set of color filters and varying levels of measurement noise, indicated in the legends by the corresponding signal to noise ration (SNR) (for additional details see [25]). If the FOM is used as a design metric, it is desirable that the relation between the FOM and the perceptual color error as quantified in $\triangle E^*_{ab}$ units follow a smooth monotonic curve so that devices designed to optimize the FOM also result in a small colorimetric error in practical applications. From the plots, in Fig. 1, we see that for the comprehensive FOM, the points in this case are almost ideally distributed, lying along a rather well defined smooth monotonic curve, whereas for the other alternative FOMs this is not so[2]. The agreement is particularly good for values of the comprehensive FOM close to 1, which represents the region of greatest interest in design optimization scenarios.

The advantage of the comprehensive FOM is apparent from the above comparisons, as it was in the original publication on this work [25]. In keeping with the theme of this paper, our objective here is to highlight how the synergistic interplay between physics and mathematics contributes to this advantage. From the vignette we presented of the overall framework, it is apparent that both physics, particularly psycho-physics, and mathematics play a key role in arriving at the powerful comprehensive FOM. The colorimetric representation and the perceptual nonlinearity represented by $\mathcal{F}()$ model the physics and the elegant mathematical tool of local linearization using the Taylor series representation

[2] A criticism of the evaluation methodology can be made on the grounds that the comprehensive FOM is designed to infact approximate $\triangle E^*_{ab}$ and therefore the comparison with $\triangle E^*_{ab}$ is unfair. This criticism can be met, however, with the counter that alternative color spaces or color difference metrics that may be shown to offer better agreement with perception in a specific application can also be readily integrated into the framework through an appropriate choice of the transformation $\mathcal{F}()$.

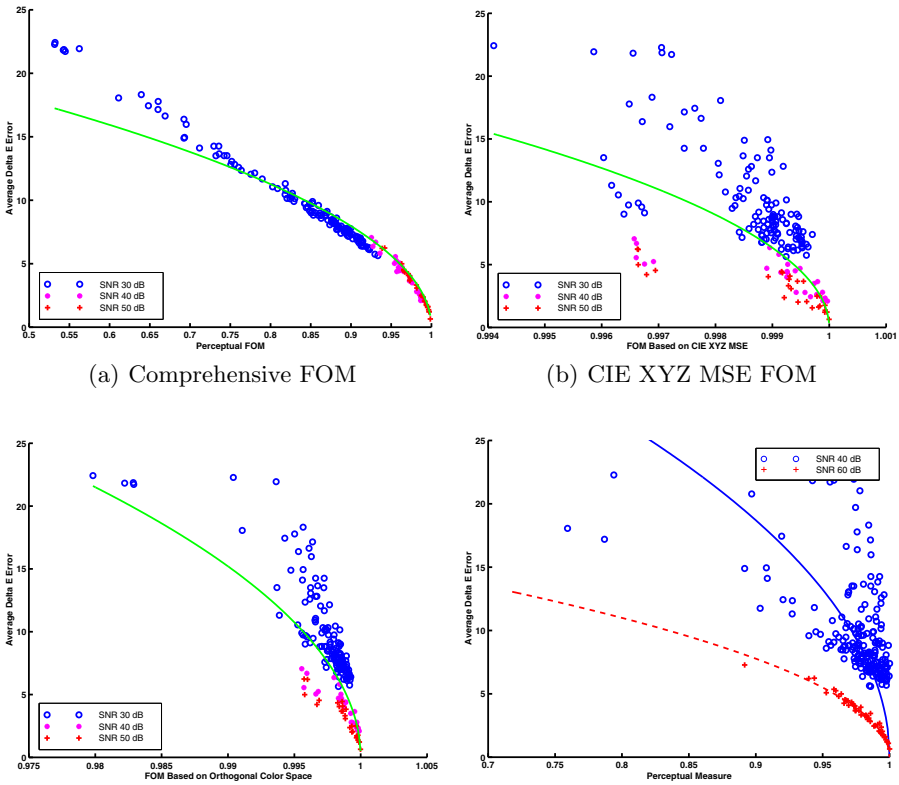

(a) Comprehensive FOM (b) CIE XYZ MSE FOM

(c) Orthogonal tristimulus FOM (d) Perceptual measure

Fig. 1. Correlation between CIELAB $\triangle E^*_{ab}$ along the abscissa and (a)Comprehensive FOM, (b) CIE XYZ MSE FOM, (c) Orthogonal tristimulus FOM, and (d) Perceptual measure. A monotone one-to-one relation is desirable for use as a design objective function. The graphs in this figure are adapted from [25].

makes the rest of the analysis feasible, particularly allowing us to compute in closed form the optimal calibration transform and the corresponding color error that forms the basis of our figure of merit framework. The CIE XYZ MSE FOM models only part of the physics of the problem dealing with color representation and adopts the mathematically simplest approach to the problem, allowing a solution without requiring the mathematical sophistication of local linearization. It offers rather poor performance for two reasons. First, the errors in CIE XYZ space do not correlate well with perception. Second, the CIE XYZ MSE FOM also ignores the mathematical correlations between the CIE XYZ coordinate representations for colors. The Orthogonal tristimulus FOM addresses the second of these limitations by orthogonalizing the tristimulus space in order to eliminate the mathematical correlations but continues to ignore the first limitation and

therefore offers only modest improvements over the CIE XYZ MSE FOM. The Perceptual measure on the other hand incorporates the (psycho)-physics of perception using the elegant mathematical framework of local linearization but is still divorced from part of physics because it fails to account for inevitable measurement noise. Thus in the mathematically idealized setting of a 60 dB SNR, it offers good agreement with color errors but under even modest degradation at a 40 dB SNR, it correlates rather poorly with perceived color errors. These limitations of the alternate FOMs therefore highlight that the advantage of the comprehensive FOM indeed arises from the combined strengths of the physical modeling and the mathematical analysis supporting our paper's eponymous claim.

4 Separation Estimation from Scanned Color Halftones

As our second case study, we consider an ingredient of our recent work [17]. on extending phase modulation watermarks for monochrome halftones [16] to four color clustered-dot halftone prints. The problem setting for this example is as follows. There exist a number of known methods that allow for embedding of invisible watermark patterns in monochrome clustered-dot halftone images as phase modulation of the halftone dots, where the embedded patterns can then be revealed by overlaying the printed halftone image with a suitably designed physical or simulated transparency mask decoder [10, 16, 26]. These methods, however, do not directly generalize to color prints using the common cyan (C), magenta (M), yellow (Y), and black (K) clustered-dot halftone separations. While the embedding of the watermarks in the individual C, M, Y, and K separations can readily follow the monochrome embedding methodology, the separations are overlaid in the print and cannot be readily separated from conventional red (R), green (G), and blue (B) scans. This problem is highlighted in Fig. 2. The black (K) colorant absorbs uniformly across the spectrum and, thus, the K halftone appears in all three of scanner RGB channels. Also the so-called "unwanted absorptions" of the CMY colorants also cause cross-coupling, i.e., C, M, and Y halftone separations not only appear in the scan R, G, and B channels that complement their spectral absorption bands, respectively, but also in the two other channels as well.

The problem in Fig. 2 seems rather difficult to address from purely a mathematical or physical perspective. Mathematically, the problem of estimating four separations from three scanner channels constitutes an under-determined problem that does not admit a unique solution and therefore offers no guarantees of discovering the correct solution. From a purely physical perspective, the absorptions of the K colorant across the spectrum and the unwanted absorptions indicate that the individual R, G, and B channels cannot directly isolate a single separation. However, as we illustrate in the sequel, and as described in greater detail in [17], the combination of physical insight with mathematical analysis does indeed lead to an effective solution whereby the four color separations can be estimated, which in turn enable per separation phase modulation halftone watermark embedding.

(a) RGB scan of CMYK halftone (b) Scan R channel (c) Scan G channel (d) Scan B channel

Fig. 2. RGB scan of a printed image that was divided into 4 stripes, where the stripes from left to right contain only C, M, Y, and K colorants, respectively. K colorant can be consistently observed in all scan channels and cross-coupling between C, M, and Y colorant halftone separations can also be clearly seen in the scan R, G, and B channels. Figure reproduced from [17].

For our description, we assume an input contone CMYK image $I_{C,M,Y,K}(x, y)$ that is typically obtained by transforming a device-independent colorimetric representation of the image to the device-dependent CMYK values via a set of color conversions [22, 30], where (x, y) denotes the spatial coordinates. Each separation is then halftoned to obtain a corresponding binary valued halftone separation $I_i^h(x, y)$, where i is one of C, M, Y, or K and rotated clustered-dot halftone screens are utilized for the four separations as is common in lithographic/electrophotographic printing. A spatial watermark pattern w_i is potentially also embedded within $I_i^h(x, y)$ using phase modulation as outlined, for example, in [16]. We adopt the convention that the values 1 and 0 for $I_i^h(x, y)$ correspond, respectively, to whether ink/toner i is, or is not, deposited (or estimated to be deposited) at the pixel position (x, y).

A scan $I_{R,G,B}^s(x, y)$ of the printed image is obtained using a conventional RGB scanner. As previously indicated, coupling between the different colorant halftones is inevitable in the scanned RGB image. Figures 3(a)–(d) show enlarged views of a region from the digital M halftone separation, digital CMYK halftone separation overlay, scanned RGB image, and scan G channel of an image used in our experiments. The M halftone colorant is complementary to the G channel, but the G channel scan clearly displays within it not only the halftone structure of the desired M separation, but also undesired halftone structures for the C, Y, and K separations with varying intensities that arise from the absorption of these colorants in the G scanner channel band.

To develop an effective solution to estimate C, M, Y, and K, halftones from the R, G, and B scans, we begin with the physical insight into the halftone process provided by the mathematical tool of Fourier analysis: the individual colorant halftone images are, phase modulation notwithstanding, narrow-band bandpass images comprised of components located on the fundamental halftone periodicity frequencies and at integer multiples thereof. By employing a suitable rotated halftone configuration, we can ensure that the fundamental halftone frequencies of the separation and their lower order harmonics do not coincide. The individual colorant separation halftones can then be separated by suitable

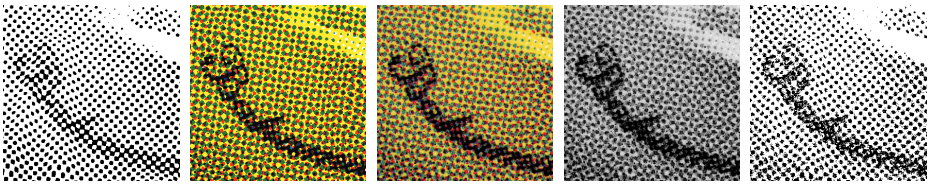

(a) $I_M^h(x,y)$ (b)$I_{CMYK}^h(x,y)$ (c) $I_{R,G,B}^s(x,y)$ (d) $I_G^s(x,y)$ (e) $\hat{I}_M^h(x,y)$

Fig. 3. Subfigure (a) shows enlarged view of a region from the digital M halftone separation of *Hats* halftone image used in our experiments, subfigure (b) shows the same region from the digital CMYK halftone overlay, subfigure (c) shows approximately the same region from the RGB scanned color halftone print, subfigure (d) shows the region from the G channel image of the scanned print showing the couplings between the halftone structures of M and C, Y, and K separations, and subfigure (e) shows the region from the M halftone estimate obtained using the methodology of [17]. Figure reproduced from [17].

filtering in the spatial frequency domain. In order to appreciate this idea, we show in Fig. 4 an enlarged view of the low frequency region for log-magnitude Fourier spectrum of the G channel image from which a section was previously shown in the spatial domain in Fig. 3(d). The fundamental frequencies corresponding to the halftones are labeled in this figure and the inter-color interference that we noted in the spatial domain can also be observed in the frequency domain. The Fourier spectrum exhibits peaks not only about the fundamental frequency vectors (and higher-order harmonics) of the M separation, but also at the fundamental frequency vectors of C, Y, and K separations, and moiré frequencies. However, observing that the primary peaks for rotated clustered-dot screens occur at different (2-D) spatial frequencies, we can also see that these and other unwanted frequency components that do not overlap with the fundamental frequency of a desired halftone can be eliminated by spatial filtering. By suitably designing the rotated halftone configuration so that the fundamental frequencies and the lower-order harmonics for each halftone screen do not coincide with those for any other halftone screen, we can estimate the halftones by employing spatial filtering.

The spatial filtering based methodology encounters some inaccuracies because in the reflectance domain of R, G, B scanner signals, the halftone separations combine multiplicatively causing part of the power in a halftone separation to be transferred to the inter-colorant moiré frequencies via the unwanted colorant interactions. This power transfer and loss of accuracy can be minimized by employing a physically-motivated mathematical model of the print and scan process that leads to an alternate transform domain representation where the combination of halftone separations is better approximated by a linear model. Specifically, if the colorants are modeled as transparent colorants obeying the the Beer-Bouguer law [7, Chap. 7] or the transparent formulation of Kubelka-Munk theory [7, Chap. 7] and the scanner responses are modeled as Dirac delta impulse

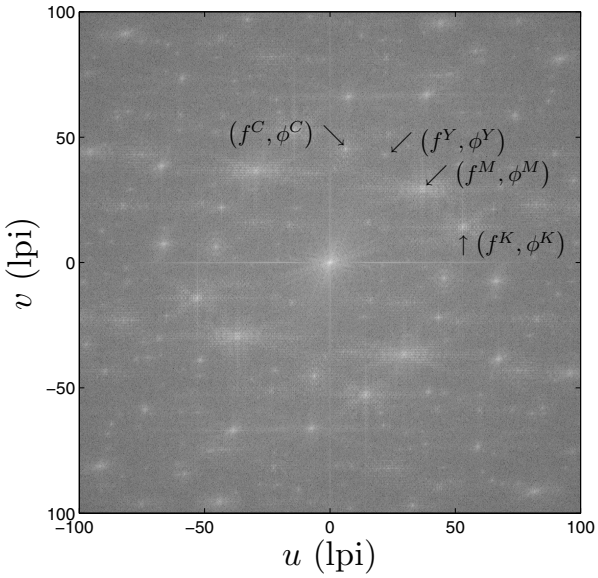

Fig. 4. Enlarged view of the log-magnitude Fourier spectrum of the G channel of the scanned *Hats* halftone print used in our experiments. For illustration purposes, the frequencies of the constituent halftone separations are indicated by arrow and text labels. Figure reproduced from [17].

functions approximating narrow band responsivities, then we can show that [17] the density for the kth channel scan is obtained as

$$d_k(x,y) \stackrel{\text{def}}{=} -\log_{10}\left(\frac{I_k^s(x,y)}{I_k^s(W)}\right) \tag{10}$$

$$= \sum_{i\in\{C,M,Y,K\}} d_k^i I_i^h(x,y), \tag{11}$$

where k denotes one of R, G, or B, $I_k^s(W)$ is the scanned image value corresponding to the paper substrate in the kth color channel and d_k^i is the optical density of the ith colorant layer in the kth scanner channel. Observe that this model is linear in the halftone separations $I_i^h(x,y)$, $i \in \{C,M,Y,K\}$ and therefore avoids avoids inter-separation moiré. Therefore, prior to spatial filtering, the halftone separations are converted into the optical density domain using the mathematical transformation indicated in (10). Even though we recognize that the model used here is an extremely idealized approximation, use of the model provides an improvement over an alternate ad-hoc approach [17].

In actual implementation of the scheme for separation of halftones, additional attention to detail is required to robustly handle all four of the separations. We refer the reader to [17] for details, only mentioning here that we develop a sequential estimation scheme guided by physical intuition; the K colorant is estimated

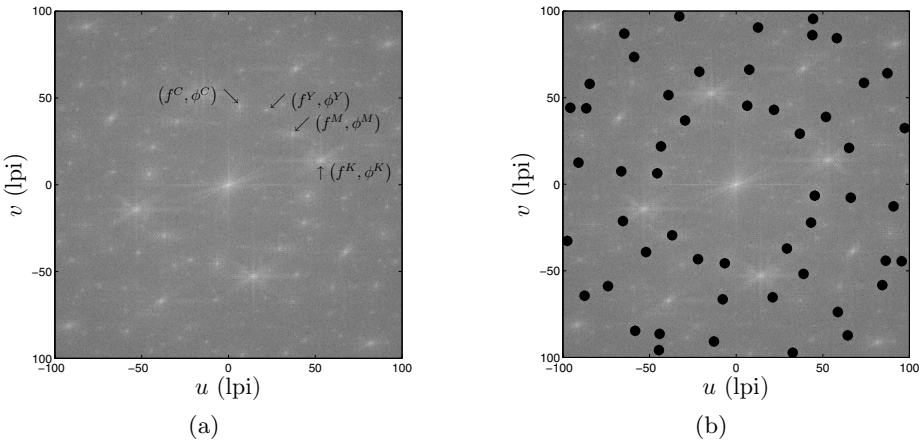

Fig. 5. Spatial filtering for estimation of K halftone $I_K^h(x)$. Subfigure (a) shows enlarged view of the log-magnitude Fourier spectrum of $d_K(x, y)$ for the scanned *Hats* print used in our experiments and subfigure (b) illustrates the elimination of unwanted frequency components of C, M, and Y halftone separations using the narrow-band band-reject filters. Figure reproduced from [17].

first using combined information from the R, G, and B scan channels, followed by an estimation of the C, M, and Y halftones using the complementary R, G, and B, scans and the already obtained estimate for the K colorant halftone. The spatial filtering process for the estimation of the K colorant separation is shown in Fig. 5, where we show the elimination of unwanted frequency components of C, M, and Y halftone separations using the narrow-band band-reject filters.

For purpose of visual assessment, enlarged views of the original CMYK halftone separations and their estimates from a region in one image (also referred to as the *Hats* image in this paper) are shown in Fig. 6. Note that the digital halftone separations undergo a variety of distortions in the printing process and therefore do not exactly correspond to the true printed halftones. Given this inherent variability, the estimates are quite good and enable effective detection of per separation halftone watermarks embedded using phase modulation[3].

The effectiveness of the scheme presented for the estimation of four CMYK halftone separations from three RGB scans is apparent from the results we highlighted above and further substantiated in the original publication on this work [17]. It should be apparent from our presentation of this case study that, just as it was necessary in our last case study example, the synergistic combination of physical intuition with mathematical analysis tools enables a novel solution to a problem that seemed, in our initial analysis, insoluble by purely physical or mathematical means.

[3] Because the application is not our focus here, we refer the reader to [17] for results demonstrating watermark detection from the separations obtained.

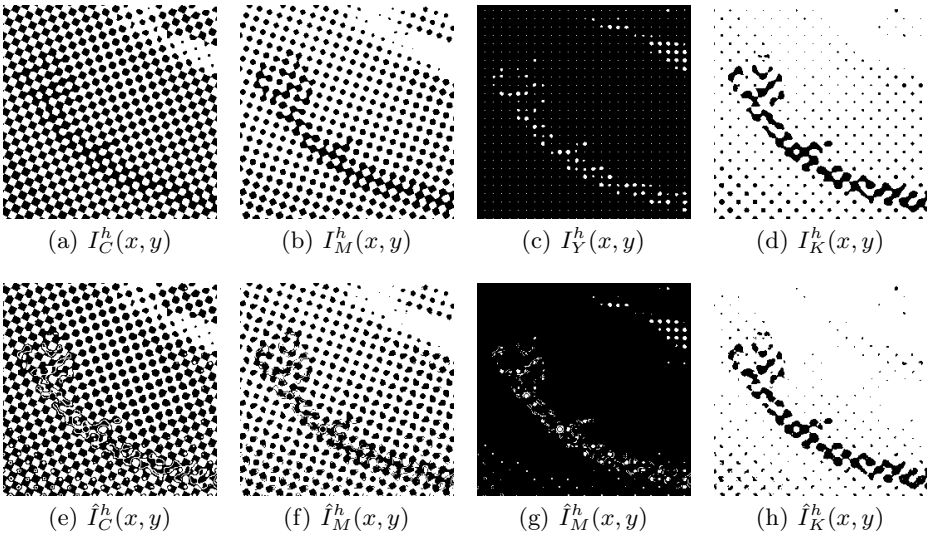

(a) $I_C^h(x,y)$ (b) $I_M^h(x,y)$ (c) $I_Y^h(x,y)$ (d) $I_K^h(x,y)$

(e) $\hat{I}_C^h(x,y)$ (f) $\hat{I}_M^h(x,y)$ (g) $\hat{I}_M^h(x,y)$ (h) $\hat{I}_K^h(x,y)$

Fig. 6. Enlarged view of the digital halftone separations (subfigures (a)–(d)) from a region in the *Hats* image and the corresponding estimates (subfigures (e)–(h)) obtained using the differences in spatial periodicity and colorant spectra.Figure reproduced from [17].

5 Summary and Discussion

Our case studies illustrated how novel and sometimes non-intuitive solutions to problems in color imaging systems can be determined by using suitable physical models and mathematical tools. As we note in the remarks for each of our case studies, in both cases, the synergistic combination of physical insight with the analytical tools of mathematics is what makes the solutions effective and powerful, supporting our assertion that in color imaging, Physics ∪ Math > Physics + Math.

We must also remark here that real-world color imaging systems and color perception rarely adhere strictly to idealized mathematical models. Approximations are therefore often necessary for making mathematical analysis tractable and useful. Both our examples also illustrate this approximation process. For obtaining the comprehensive FOM, we approximate the nonlinear transformation from CIE XYZ to CIE LAB via a local linearization and for the halftone separation case study we approximate the combination of colorant transmittances in print by using a linear in density model that conforms better with the linear Fourier domain filtering framework for separation. Despite the approximations, the models demonstrate their utility when the approximations are also guided by physical insight to align closely with the analysis. Of course, overly simplistic mathematical models that are not physically justified can also result in poor results. This is the situation, for instance, in our first case study, when MSE in CIE XYZ space is utilized as a metric for perceptual color error.

Our presentation in this paper continues the broader "Physics $\cup$ Math $>$ Physics + Math" philosophical theme that was previously initiated in [23]. The later perspective in time for the current paper allows us to draw our illustrative examples from a larger body of work, including several projects undertaken in the intervening time. The two illustrative case studies that we have chosen for supporting the hypothesis in this paper's title are drawn from our own research because these examples are most familiar to us and because the corresponding published material is readily accessible to us. The research for the individual case studies presented here has previously been published in more detailed individual contributions on figures of merit for color recording devices [25] and on color CMYK halftone separation estimation from RGB scans for color halftone watermarking applications [17]. The exposition in the present paper borrows heavily from these prior publications. Our previous paper on the broader theme [23] included as examples, work on show-through correction [20] and set-theoretic estimation for subtractive color [18, 19]. We encourage readers whose interests may have been stimulated by specific examples, to follow the relevant publications for additional information and details.

Clearly, we cannot and do not claim to monopolize the broader underlying theme of this paper; a far larger set of equally good and perhaps better examples can be found in the works of other researchers. The happy union between Physics and Mathematics underlies not only the origins of color science and numerous pre-existing applications in color imaging, but continues to be a key enabler of future innovations in color imaging systems. Moreover as we indicate in the opening paragraph of the introduction, the theme of the paper is also a subset of the broader idea that pervades a wider arena of applications, where solution methodologies are most successful when they combine the insight offered by the physics underlying the problem with the mathematical framework and tools inherent in digital signal and image processing [8].

Acknowledgments. The examples used in this invited paper are drawn from research on which I have worked over a number of years. The research would not be feasible or complete without my collaborators on these and other research projects. I would like to acknowledge my gratitude to these colleagues, both the direct contributors that are indicated in the associated citations and the indirect contributors who have provided thought-provoking discussions and a lively environment for research. I would also like to thank the various funding agencies and companies that have supported my research at the University of Rochester.

References

1. CIE: Colorimetry. CIE Publication No. 15.2, Central Bureau of the CIE, Vienna (1986), the commonly used data on color matching functions is available at the CIE web site at `http://www.cie.co.at/`
2. Cohen, J.B., Gibson, W.A.: Vector model for color sensations. J. Opt. Soc. Am. 52(6), 692–697 (1962)

3. Dubois, E.: The structure and properties of color spaces and color image spaces. Synthesis Lectures on Image, Video, and Multimedia Processing 4(1), 1–129 (2009)
4. Franklin, G.F., Powell, J.D., Emami-Naeini, A.: Feedback Control of Dynamic Systems, 6th edn. Prentice Hall, Englewood Cliffs (2009)
5. Golub, G.H., Loan, C.F.V.: Matrix Computations, 2nd edn. The Johns Hopkins University Press, Baltimore (1989)
6. Grassmann, H.G.: Zur theorie der farbenmischung. Poggendorf. Annalen der Physik und Chemie 89, 69–84 (1853); translation titled Theory of compound colors. Philosophic Magazine 4(7), 254–264 (1854), reprinted in [11,12]
7. Grum, F., Bartleson, C.J. (eds.): Optical Radiation Measurements: Color Measurement, vol. 2. Academic Press, New York (1980)
8. Haykin, S.: Signal processing: where physics and mathematics meet. IEEE Sig. Proc. Mag. 18(4), 6–7 (2001)
9. von Helmholtz, H.L.F.: Physiological Optics (1866), extracts reprinted in [11]
10. Knox, K.T., Wang, S.: Digital watermarks using stochastic screens. In: Beretta, G.B., Eschbach, R. (eds.) Proc. SPIE: Color Imaging: Device Independent Color, Color Hardcopy, and Graphic Arts II, vol. 3018, pp. 316–322 (February 1997)
11. MacAdam, D.L. (ed.): Sources of Color Science. MIT Press, Cambridge (1970)
12. MacAdam, D.L. (ed.): Selected Papers on Colorimetry-Fundamentals. SPIE Optical Engineering Press, Bellingham (1993)
13. Magnus, J.R., Neudecker, H.: Matrix Differential Calculus with Applications in Statistics and Econometrics. Wiley, Chichester (1988)
14. Maxwell, J.C.: The diagram of colors. Transactions of the Royal Society of Edinburgh 21, 275–298 (1857), reprinted in [11,12]
15. Maxwell, J.C.: Theory of compound colors and the relations to the colors of the spectrum. Proc. of the Royal Society of London 10, 404–409 (1860), reprinted in [11,12]
16. Oztan, B., Sharma, G.: Continuous phase-modulated halftones. IEEE Trans. Image Proc. 18(12), 2718–2734 (2009), `http://www.ece.rochester.edu/~gsharma/papers/OztanSharmaContinPhaseModTIPDec2009.pdf`
17. Oztan, B., Sharma, G.: Per-separation clustered-dot color halftone watermarks: Separation estimation based on spatial frequency content. J. Electronic Imaging 19(4), 043007–1–22 (2010), `http://www.ece.rochester.edu/~gsharma/papers/OztanPerSepColrHTWMFreqSepJEI043007.pdf`
18. Sharma, G.: Set theoretic estimation for problems in subtractive color. Color Res. Appl. 25(4), 333–348 (2000), `http://www.ece.rochester.edu/~gsharma/papers/subcolpocsCRNA2000.pdf`
19. Sharma, G.: Target-less scanner color calibration. J. Imaging Sci. and Tech. 44(4), 301–307 (2000), `http://www.ece.rochester.edu/~gsharma/papers/ntargcaljist00.pdf`
20. Sharma, G.: Show-through cancellation in scans of duplex printed documents. IEEE Trans. Image Proc. 10(5), 736–754 (2001), `http://www.ece.rochester.edu/~gsharma/papers/showthuip01.pdf`
21. Sharma, G.: Color fundamentals for digital imaging. In: Digital Color Imaging Handbook [22], chapter 1
22. Sharma, G. (ed.): Digital Color Imaging Handbook. CRC Press, Boca Raton (2003)
23. Sharma, G.: Imaging Arithmetic: Physics u Math > Physics + Math. In: Eschbach, R., Marcu, G.G. (eds.) Proc. SPIE: Color Imaging X: Processing, Hardcopy, and Applications, vol. 5667, pp. 95–106 (January 2005), `http://www.ece.rochester.edu/~gsharma/papers/imagphysmathei05.pdf`, invited Paper

24. Sharma, G., Trussell, H.J.: Digital color imaging. IEEE Trans. Image Proc. 6(7), 901–932 (1997), http://www.ece.rochester.edu/~gsharma/papers/dciip97.pdf
25. Sharma, G., Trussell, H.J.: Figures of merit for color scanners. IEEE Trans. Image Proc. 6(7), 990–1001 (1997), http://www.ece.rochester.edu/~gsharma/papers/fomip97.pdf
26. Sharma, G., Wang, S.: Show-through watermarking of duplex printed documents. In: Delp, E.J., Wong, P.W. (eds.) Proc. SPIE: Security, Steganography, and Watermarking of Multimedia Contents VI, vol. 5306, pp. 670–684 (January 2004), http://www.ece.rochester.edu/~gsharma/papers/showthruWMei2004.pdf
27. Sharma, G.: Color scanner characterization, performance evaluation, and design. Ph. D. dissertation, North Carolina State University, Raleigh, NC (August 1996)
28. Wyszecki, G., Stiles, W.S.: Color Science: Concepts and Methods, Quantitative Data and Formulae. John Wiley & Sons, Inc., New York (1982)
29. Young, T.: On the theory of light and colors. Philosophical Transactions of the Royal Society of London 92, 20–71 (1802), extracts reprinted in [11,12]
30. Yule, J.A.C.: Principles of color reproduction, applied to photomechanical reproduction, color photography, and the ink, paper, and other related Industries. Wiley, New York (1967)